High-Repetition-Rate Ultrafast Fiber Lasers for Material Processing

Hamit Kalaycıoğlu 🆔, Parviz Elahi 🆔, Önder Akçaalan, and Fatih Ömer Ilday 🆔

(Invited Paper)

Abstract—**Ultrafast lasers operating at high repetition rates, in particular the GHz range, enable new possibilities in laser-material processing, particularly accessing the recently demonstrated ablation-cooled regime. We provide a unified perspective of the unique opportunities created by operating at high repetition rates together with our efforts into the development of enabling laser technology, including new results on further scaling up the capabilities of the laser systems. In order to access GHz repetition rates and microjoule-level pulse energies without requiring kilowatts of average power, we implement burst-mode operation. Our results can be grouped into two distinct directions: low- and high-power systems. Pulsed pumping is employed in the later stages of low-power systems, which have low burst repetition rates to achieve high pulse energies, whereas the technique of doping management is developed for the continuously pumped power amplifier stage of high power systems. While most of the developments have been at 1-μm wavelength range due to the relative maturity of the laser technology, we also report the development of Tm-fiber lasers around the 2-μm region specifically for tissue processing and laser-surgery applications.**

Index Terms—**Fiber lasers, high repetition rate lasers, burst mode, ultrafast fiber lasers, lasers for material processing, ablation-cooled laser-material removal.**

I. INTRODUCTION

FIBER lasers constitute a major area of interest in the field of laser research as versatile sources of continuous wave and pulsed laser radiation. Fiber integrated architecture specifically attracts attention since light guided inside flexible fibers throughout the system enhances stability and robustness as well as allowing compact structure [1]–[4]. As so, fiber architecture holds a great potential for material processing with ultrashort pulses, which produces precise ablation with minimal thermal damage to the surroundings of the target material. While ultrafast fiber laser technology has matured to a good extent under intensive research in the past decade, two major drawbacks have remained for material processing with ultra-short pulses; relatively low material removal speeds and complexity of associated laser technology, which arises, in part, due to requiring both high pulse energies and ultrashort pulse durations.

We have recently discovered a new regime of ultrafast laser material processing which we call ablation-cooled material removal that overcomes the deficiencies and unleashes its potential for industrial and medical applications [5]. In this regime, cooling of the material takes place simultaneously with ablation under the bombardment of pulses repeated with a period short enough that relatively limited heat diffusion can take place from the targeted area to the surroundings. The targeted material heats with each successive pulse up to the critical temperature required for the evaporative removal, and the ablation takes place removing a major portion of the thermal energy localized at the targeted spot. In [5], the physics of this regime is explained with a toy model which predicts the experimental results very accurately. The parameters, material thermal relaxation time τ_0 and pulse repetition period τ_R play critical roles in this model which is based on the exposed material evaporating at a critical ablation temperature T_c. The instantaneous temperature rise ΔT produced by each incident pulse on the material builds up and reaches right after n pulses to $T_n = T_0 + (n - 1)\frac{\Delta T}{\sqrt{(1 + \frac{\tau_R}{\tau_0})}} + \Delta T$. Here $\frac{\Delta T}{\sqrt{(1 + \frac{\tau_R}{\tau_0})}}$ is the residual temperature rise from each pulse after the instantaneous surge relaxes with τ_0, characteristic of the material. The critical threshold for ablation is reached when T_n exceeds T_c. In the traditional laser material processing regime with low repetition rates, the delay between each pulse is substantially longer than the relaxation time, and each pulse has an individual effect, and residual temperature rise is negligible so $T_n = T_0 + \Delta T$. Hence each pulse has to have enough energy to raise the material to the critical temperature; however, in the ablation cooling regime where τ_R for high repetition rate pulses is comparable or less than τ_0, the pulses have a cumulative effect and ablation starts when for the mth pulse $T_m = T_0 + (m - 1)\frac{\Delta T}{\sqrt{(1 + \frac{\tau_R}{\tau_0})}} + \Delta T > T_c$. So, for a train of N pulses large enough for the cumulative effect to occur ($N >> m$), ablated volume can be stated as $V_{ablated} = \beta(N - m)E_p$, β representing a proportionality constant and E_p the energy per pulse.

H. Kalaycıoğlu, P. Elahi, and Ö. Akçaalan are with the Department of Physics, Bilkent University, Ankara 06800, Turkey (e-mail: hamitkal@bilkent.edu.tr; pelahi@fen.bilkent.edu.tr; akcaalan@bilkent.edu.tr).

F. Ö. Ilday is with the Department of Electrical and Electronics Engineering and the Department of Physics, Bilkent University, Ankara 06800, Turkey (e-mail: ilday@bilkent.edu.tr).
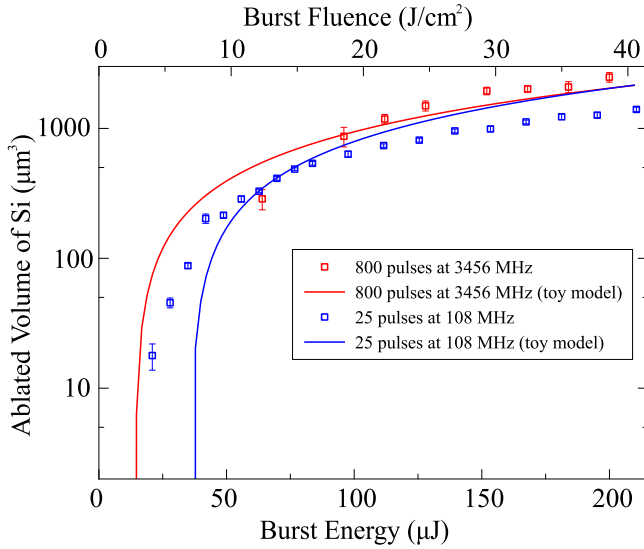
Fig. 1. Volumes Si ablated by a single burst of pulses as a function of total incident energy for two different intraburst repetition rates and the predictions of the toy model for these repetition rates in the ablation-cooled regime (solid lines). Reproduced with permission from [5], ©2016 Nature Publishing Group.

In this regime, the heat that diffuses into the material is given by

$$E_{heat} = \alpha(T_c - T_0)(1 - \frac{1}{\sqrt{(1 + \frac{\tau_R}{\tau_0})}})(N - m)E_p$$

$$+ \alpha(\Delta T - \frac{\Delta T}{\sqrt{(1 + \frac{\tau_R}{\tau_0})}})mE_p,$$

where α is the thermal diffusivity of the material. This indicates that as the repetition rate increases, the energy transferred into the material diminishes totally in the limit of zero delay between pulses, while on the other end with the delay $\tau_R >> \tau_0$ the transmitted energy becomes $E_{heat} = \alpha(\Delta T)NE_p = \alpha(T_c - T_0)$ NE_p where each pulse raises the material temperature to T_c. Of course, it must be emphasized that the scaling of the repetition rate to higher and higher values is expected to terminate at a finite value, limited, ultimately, by the finite time it takes for the ablation process itself to take place. So, this is one of the two main predictions of the model which was demonstrated in experiments on numerous materials showing that the processed material heats less for higher repetition rates when the inter-pulse period becomes short compared to the relaxation time specific to that material [5]. The other prediction is demonstrated in Fig. 1 on Si samples with experimental data and calculated curves based on toy model, and states that the pulse energy can be scaled down while ablation efficiency is preserved as long as the number of pulses incident is increased in the same proportion. Here, the ablation efficiency is shown even to improve with an intraburst repetition rate of 3.5 GHz relative to 100 MHz while all other parameters such as incident fluence and energy per spot are kept constant.

In order to investigate the potential of ultrafast laser-material processing with ultra-high repetition rates, which eventually lead us to the development of the ablation cooling concept, we implemented the burst-mode operation. This mode of opera-

tion consists of pulses repeated at high repetition rates located inside groups, called bursts, which are themselves repeated at much lower rates. The low duty cycle leads to the attainable output powers which circumvents the impractical requirements for laser systems to produce high-energy (at least, at the microjoule level) pulses continuously at very high repetition rates. As a matter of fact, burst-mode laser systems have been in use for a while in niche applications such as accelerators [6], [7], combustion diagnostics [8], flow measurements in aerodynamics [9], Thomson scattering experiments [10], pulsed laser deposition [11], photoacoustic microscopy [12]. More recently, they have also been attracting attention as tools for efficient material processing [13]–[16] since it was demonstrated as a strong alternative by Marjoribanks and colleagues [17].

Seeing the potential and having the desire to investigate high repetition rates in material processing, we embarked on the development of burst-mode fiber laser systems. Up to then, solid state laser systems were used in burst-mode operation, and they were not optimized for such mode of operation. Fiber systems offered the stability for long term operation in processing experiments. They further held the potential of versatility of variable intraburst repetition rate via integrable repetition rate multipliers and variable burst repetition rates via fiber coupled modulators. In 2011, we demonstrated the first fiber laser explicitly designed to operate in the burst mode [18] and continued our development efforts of laser systems operating at 1 μm with high intraburst repetition rates in two main directions: low power systems with low burst repetition rates [18]–[21] which yield low effective repetition rates (burst repetition rate x number of pulses per burst < MHz), and high power systems with high repetition rates operating in either continuously pulsed or burst mode [22]–[24]. In the meantime, Limpert et al. demonstrated an impressively high-energy (58 mJ) rod-fiber type burst-mode amplifier [25] and Li et al. demonstrated bursts with controllable number of pulses from a mode-locked Yb-doped all fiber laser system [26]. And very recently, we have begun to develop Tm-doped ultrafast fiber burst-mode systems operating at 2 μm, with a purpose to investigate tissue processing in the ablation-cooled material removal regime [27]. This is a switch from the low absorption region of 1 μm, where ultrafast processing is dependent on nonlinear ablation nearly totally, to a region where laser tissue interaction will be enhanced strongly by the local absorption peak of water at 1.94 μm [28], especially for water-rich soft tissues. This report includes, first a discussion on the development of low power systems followed by the high power systems, both operating at 1 μm, and finally, a summary of our most recent work on the Tm-doped burst-mode system.

II. LOW-POWER SYSTEMS

The general configuration of the high repetition rate systems that we have developed is the fiber-integrated cascaded amplification [29], [30] seeded by an all-normal dispersion (ANDi) laser oscillator [31] with a pulse picker acousto-optic modulator (AOM) placed within the amplifier chain to transform the uniform mode-locked pulse train into the burst format. The distinct feature of low-power systems is the energy storage scheme implemented by pulsed pumping in order to obtain kHz-level burst
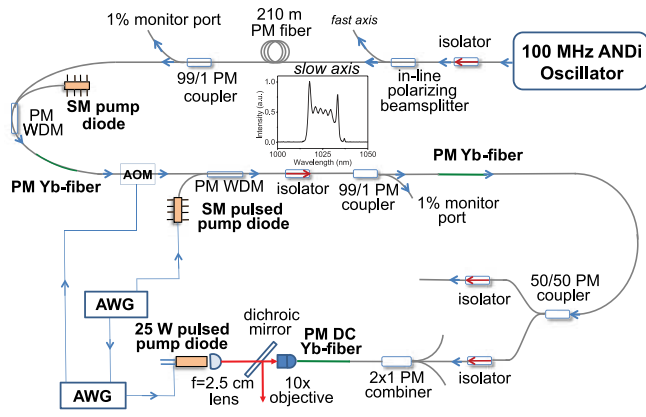
Fig. 2. Schematic diagram of the first fiber burst-mode amplifier system WDM: wavelength division multiplexer PM: polarization maintaining, SM: single-mode, DC: double-clad, AWG: arbitrary waveform generator, AOM: acousto-optic modulator. Inset: spectrum of the seed signal. Reproduced with permission from [18], ©2011 OSA Publishing Group.
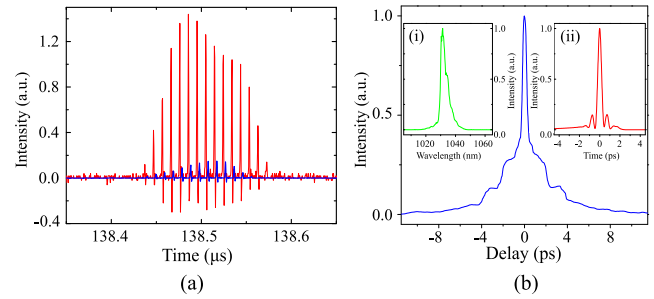

Fig. 3. (a) Performance highlights of the first fiber burst-mode system: Pulse bursts at the power amplifier input (solid, red lines) and output (dashed, blue lines) for 150 ns-long signal burst, amplified burst energy of 0.25 mJ, highest pulse energy of 27 μJ. Seed signals levels are multiplied by a factor of 20 for clarity. (b) Autocorrelation trace for the amplified bursts of (a), insets: (i) optical spectrum, (ii) pulse shape obtained from numerical simulations. Reproduced with permission from [18], ©2011 OSA Publishing Group.

repetition rates. The seed is amplified with continuous pumping before it is converted to the low-duty cycle burst train via the AOM, whereafter the average signal power drops significantly and pulsed pumping is employed.

A. First Burst-Mode Fiber Laser System

The first version of such systems formed the backbone of the high intraburst repetition rate systems with low average output power. It consisted of a 100 MHz all-normal dispersion (ANDi) oscillator seeding two stages of core-pumped fiber preamplifiers, a double-clad (DC) fiber power amplifier as well as synchronized pulse picking and pulsed-pumping electronics (Fig. 2) [18]. Two arbitrary waveform generators (AWG) are used to drive the AOM and the pulsed pump diodes. The signal to the AOM is delayed with respect to the diode drivers by an adjustable amount such that the signal burst arrives precisely at the very end of the much longer pump pulse. The AWG's allow adjustment of the durations of the pump pulses to maximize burst energy while suppressing ASE as much as possible. Also, the burst duration and the burst repetition frequency can be adjusted freely. The oscillator output is polarized with an in-line polarization beam splitter (PBS), followed by polarization maintaining (PM) components. The seed pulses, with a bandwidth of 16.5 nm, are stretched to 165 ps in 210 m-long PM fiber and amplified in a continuously pumped preamplifier to about 300 mW. After the AOM, the bursts are amplified by a pulsed pump source with a maximum peak power of 450 mW in synchrony with the signal burst.

For the power amplifier, backward pumping through bulk optics and use of a short gain fiber helps minimize the nonlinear effects and keep the gain peak around 1030 nm. The gain fiber is a highly doped Yb-fiber with a core diameter of 20 μm, core NA of 0.07 and cladding diameter of 125 μm. About 70% of the pump power is coupled into the gain fiber with a collimating lens of 2.5 cm focal length and a 10x objective. With this

system, we could obtain an average pulse energy of $\sim$20 μJ for a burst duration of 150 ns, which contained approximately 13 pulses (Fig. 3(a)). Pump pulse durations of 135 μs and 130 μs are used for the second preamplifier, and the power amplifier, respectively, and an appropriate ramp gate pulse is applied to the AOM to homogenize the pulse energies within the burst. The highest pulse energy within the burst is 27 μJ, with the total burst energy being 250 μJ, after correction for ASE. This corresponds to a pump-to-signal conversion of 13% with respect to coupled pump power and the net gain of 30 dB for the power amplifier. The ASE content in the final output is estimated to be about 2.5% via our gain simulation program and experimentally confirmed to be below 10% as determined by applying the same pump power with no signal. The nonlinear phase shift for the power amplifier at 20 μJ pulse energy level is estimated to be 10π. The amplified pulses of a maximum energy of 20 μJ are compressed by an external grating compressor to $\sim$400 fs, as inferred from the autocorrelation measurement, assuming a deconvolution factor for a Gaussian pulse (Fig. 3(b)).

B. Homogenisation of Intraburst Pulse Energy

The burst-mode laser amplifier was next developed to tackle the problem of homogenization of the intraburst pulse energy distribution and further increase burst energy [19]. During high-energy operation with pulsed pumping, depletion of the gain during the burst becomes considerable, leading to significant variation in pulse energy across the burst (Fig. 4(a)). The variation across the burst can be partially offset by modulating input burst signal (preshaping) through the AOM such that the net gain times the launched pulse energy is nearly constant. Further homogenization of the individual pulse energy inside the burst is possible by optimizing the ramp signal applied to the AOM. This advanced preshaping method was used to achieve less than 2% variation in pulse energy within the burst (Fig. 4(b)), while at the same time scaling up the individual pulse energy to 60 μJ and the burst energy to above half mJ level at 1 kHz. The present limit arises from noise in the detection electronics and could readily be reduced further with dedicated electronics design. In this upgraded version shown schematically in Fig. 5,
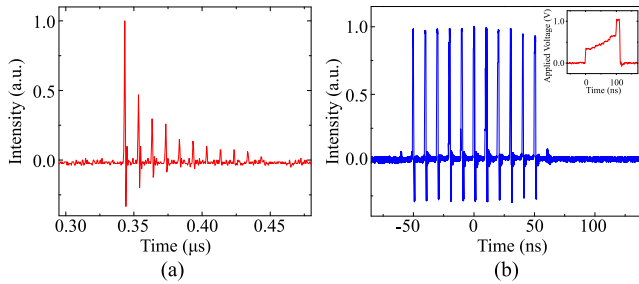
Fig. 4. Temporal profile of the amplified burst with total energy of (a) 150-μJ, with no precompensation, (b) 660-μJ, with precompensation, comprised of 11 60-μJ pulses (pulse-energy variation of $< 2\%$), inset: corresponding gate signal applied to the AOM. Reproduced with permission from [19], ©2012 OSA Publishing Group.
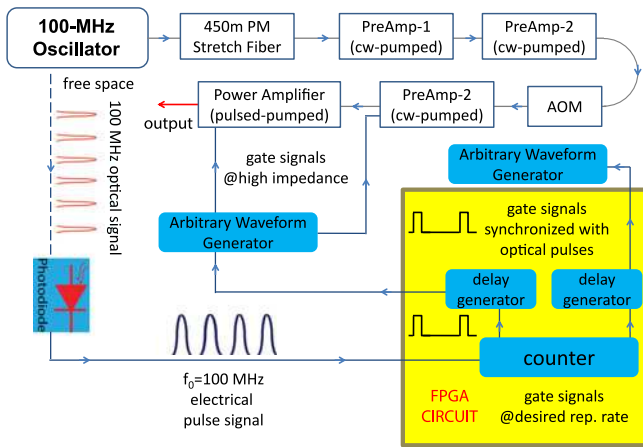

Fig. 5. Burst-mode laser amplifier system developed to produce more than half a mJ level bursts with very highly uniform intraburst energy distribution. PM: polarization maintaining, AOM: acousto-optic modulator, FPGA: field programmable gated array. Reproduced with permission from [19], ©2012 OSA Publishing Group.

210 m of stretch fiber was extended to 450 m while amplification was boosted by adding a second continuously-pumped preamplifier, and a pulse-pumped preamplifier. The longer stretching of the pulses allowed obtaining higher pulse energies. However, compression of 40 μJ pulses with 1500 line/mm grating pairs generated an effective pulse width of 1.2 ps due to the effect of residual TOD and estimated nonlinear phase shift of 16π in the power amplifier.

An in-house developed FPGA based electronics were integrated into the laser system to minimize the jitter of the pulses inside the burst and facilitate the homogenization of the energy distribution within the burst. The pulse picking and the pulsed pumping processes are both synchronized using a signal derived from the 100 MHz oscillator and managed by the field programmable gated array (FPGA) circuit. The FPGA circuit is triggered by the RF signal derived from the optical pulse train produced by the oscillator signal. This low-jitter signal [32] is low-pass filtered to retain only the fundamental frequency of 100 MHz, which is used as the internal clock signal of the FPGA, ensuring the tightest possible synchronization allowed with the hardware limitations of an FPGA. The FPGA, in turn, triggers three arbitrary waveform generators (AWG), one of

which drives the AOM and the other two provides pulses to diode drivers, which are capable of pulsed operation.

It is evident that by impressing a complex variation on the launched burst, one can obtain an arbitrarily uniform amplified pulse train at the cost of decreased efficiency, the extent of which increases for longer burst duration. To this end, we developed an iterative optimization algorithm to obtain a systematic method of pulse energy homogenization for a burst of arbitrary duration (see [19] for more details). The amplified pulse train for a modest 150-μJ burst with no precompensation in Fig. 4(a) illustrates the importance of precompensation, when compared to the 110-ns long half a millijoule burst obtained using the precompensation algorithm (Fig. 4(b)). The corresponding gate signal applied to the AOM is shown in the inset of Fig. 4(b). The measured standard deviation with respect to the mean pulse energy is $<2\%$, a remarkable improvement compared to 116% for the uncompensated case (Fig. 4(a)) with much lower energy.

C. Investigation of ASE Generation and Limits of the Burst Energy

To explore the limits of burst energy for short burst duration and hence the individual pulse energy, we upgraded the system to nine stages of amplification aiming to suppress ASE at low repetition rate while employing a chirped fiber Bragg grating (CFBG) for a pulse stretcher with a stretching ratio of $\sim$1000 (Fig. 6) [20]. The CFBG was designed to match an 1800 line/mm transmission grating. The 100-MHz oscillator seeded six stages of core-pumped fiber pre-amplifiers, a three-stage double-clad (DC) fiber power amplifier, where the first three preamplifiers located before the AOM were pumped continuously, and all the rest of six stages coming after the AOM were pulse-pumped. The power amplifier at the end of the system consisted of two forward-pumped and final one backward-pumped stage, which employed one, two and three 25-W pump diodes, respectively. Since the main limitation to burst energy arises from ASE generation in a low-repetition-rate system, ASE was carefully monitored at various stages, and the output and pulsed pumping parameters were optimized to achieve the highest signal to ASE ratio.

Investigation of the three-staged pulsed preamplifier showed that pumping the first two stages with a lower energy level and increasing it for the third stage resulted in the best combination of high burst energy and low ASE content. Compared to the performance of the single pulsed preamplifier (threshold pump energy of 16 μJ for ASE onset, pump to signal conversion of 2.5%) in the previous version of the system [18], a six-fold increase both in threshold and conversion efficiency (95 μJ and 16%, respectively) for similar ASE level has been achieved via three-stage preamplification for 100-ns bursts repeated at 1 kHz. An input signal containing short signal bursts (below 500 ns duration) and zero ASE level were used for each stage to investigate the limits to amplification and the ASE generation characteristics of the three-stage power amplifier. An overview of the results is shown in Fig. 7(a) where a similar trend of converging amplified burst energy and threshold behavior for ASE onset, a shift to a higher level (230 to 400 μJ for burst energy and 0.6 to 1.2 mJ for pump energy threshold) via cascaded
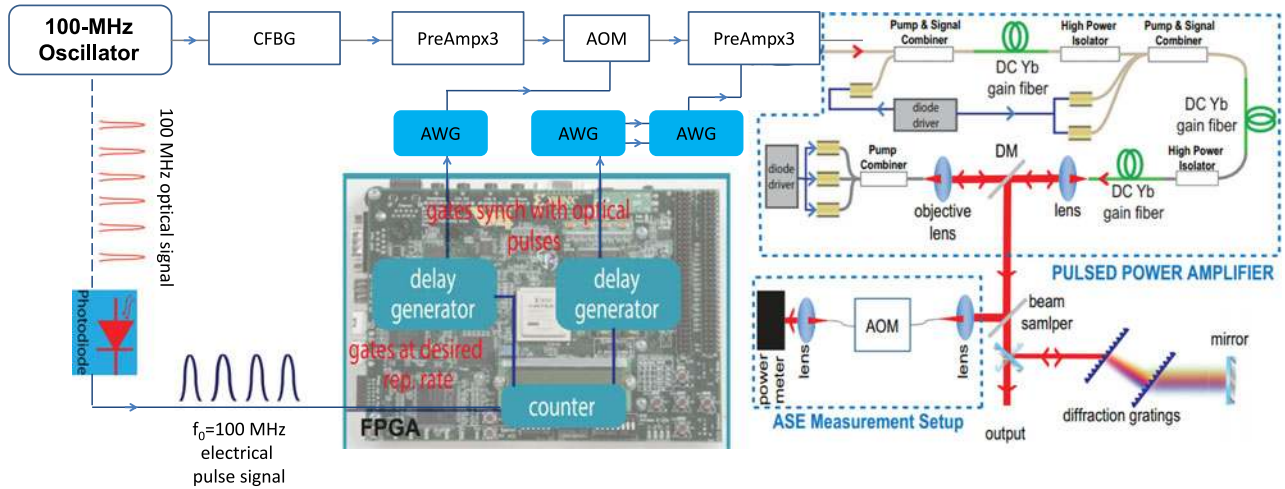
Fig. 6. Highly cascaded burst-mode laser amplifier system developed to investigate the limits of burst energy for short burst durations. CFBG: chirped fiber Bragg grating, AWG: arbitrary waveform generator, AOM: acousto-optic modulator, FPGA: field programmable gated array, DC: double-clad, DM: dichroic mirror. Reproduced with permission from [20], ©2015 OSA Publishing Group.
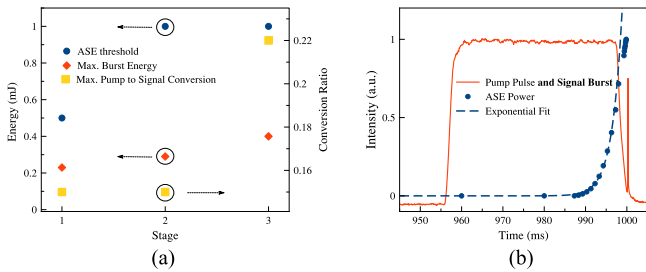

Fig. 7. (a) A summary of the performance analysis results of the three-stage power amplifier. Maximum net signal burst energy, pump energy threshold for ASE generation, pump to signal conversion ratio, for the tree stages. Note that the data for the second stage output is the result of the cumulative amplification of the first two stages. (b) Temporal characterisation of ASE generation in the case of 1.7 mJ pump pulse with 40 μs duration, amplified net burst energy of 400 μJ and 20% ASE ratio in the output. ASE generation (triangles facing down) versus time and exponential fit (dashed line) to it with the formula of $I(t) = 0.017 \times e^{(t-989)/2.43}$. Pump and signal pulses are also shown (solid line). The arrival of the signal burst at 1 ms mark can also be seen. Reproduced with permission from [20], ©2015 OSA Publishing Group.

amplification is observed. The pump-to-signal conversion efficiency, a critical parameter for a system based on energy storage, follows a similar trend in all the three stages where the conversion increases to 15% for the front stages and 22% for the final stage and degrades afterwards due to ASE growth (Fig. 7(a)). ASE generation was further characterized at the final stage of the power amplifier for the case of a pump pulse of 1.7 mJ and 40 μs duration, amplified net burst energy of 400 μJ and 20% ASE ratio in the output(Fig. 7(b)). The close exponential fit to the ASE growth yields a time constant of 2.4 μs over a period of $\sim$10 μs before the signal burst arrives and terminates once the signal burst arrives at the 1 ms mark. Since the launched signal has no ASE content, the ASE growth initiating $\sim$30 μs after the onset of pump pulse indicates a threshold of $\sim$1 mJ stored pump energy for the parameters considered here in agreement with Fig. 7(b).

Ways to suppress ASE generation further and extend the limit for burst energies from fiber amplification of short bursts (<500 ns) were also explored. First, increasing the peak pump

power significantly and reducing the pump pulse duration down to the levels comparable to or below ASE growth period ($\sim$10 μs for the conditions stated above) was tested. To this end, two 100-W pump diodes were employed at the final stage; however, our findings suggested that ASE generation for a specific fiber is dependant on threshold pump energy principally, and pump pulse duration has no measurable effect. Next, considering the 30-fold improvement in the ASE threshold with Yb 1200 20/125 DC fiber in the single stage forward pumped amplification with respect to the single-mode single stage preamplifier, a fiber with higher energy storage capacity (core/cladding dimension 30/250 instead of 20/125) was tested in the final stage of the power amplifier. At 4.5 mJ pump energy, 700 μJ net burst energy was achieved with 25% ASE level in the output for a significant improvement from the 600 μJ with 100% ASE level for the replaced PM Yb 1200 20/125 DC fiber at the same pump energy. Another possibility, adding an amplifier stage is not a viable option since limits of nonlinearity suppression, and gain filtering has been practically reached with commercially available grating size and a shrunk spectrum. Further, placing an AOM is an option, which would allow entering the final stage with higher energy. This would offer a potential improvement of 200-300 μJ, considering the limits of the front two stages. However, this would introduce added complication to the setup. Also, a free-space AOM might be required due to the large core fibers, which would spoil the all-fiber architecture. Hence, the more practical way to boost burst energy is to use the higher energy storage capacity of the fibers with larger cross sections, but not fibers with higher concentration (doping level) which increases gain for the same length of fiber used and equally supports ASE generation as well as the signal.

D. Increasing the Intraburst Repetition Rate Up To 3.5 GHz

In order to test the ablation-cooled material removal regime with important materials of high thermal diffusivity such as copper, silicon, high pulse repetition rates in the GHz range are required. As described in the Introduction section above, in this
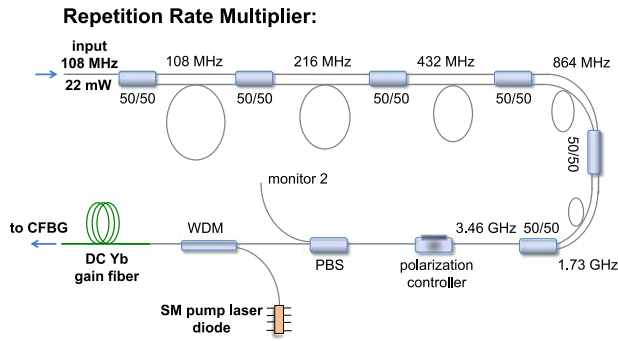
Fig. 8. Schematic diagram of the repetition rate multiplier. WDM: wavelength division multiplexer, PBS: polarization beam splitter, CFBG: chirped fiber Bragg grating, SM: single-mode. Reproduced with permission from [21], ©2016 Elsevier Publishing Group.

regime the repetition rate has to be high enough that there is insufficient time for the targeted spot size to cool down substantially by heat conduction into the rest (bulk) of the target material by the time the next pulse arrives. Hence, few GHz levels are required for materials with thermal relaxation time in the nanosecond range. To attain such high repetition levels, we implemented repetition rate multiplication with cascaded 3-dB fiber optic couplers which offer a practical solution by an integer multiplication factor of $2^{(N-1)}$, where N is the number of the couplers [33]–[35]. The seed signal from a 108-MHz fiber oscillator is converted to 3.5 GHz by a fiber-optic multiplier consisting of six cascaded 3-dB couplers as shown in Fig. 8 [21]. The output from the oscillator is transmitted to the repetition rate multiplier consisting of cascaded 3-dB couplers, where for each coupler there is a length difference between the two output arms, equivalent to a delay of half of one period of the signal repetition rate at the input of that coupler. Therefore, the repetition rate is doubled at each stage, beginning with the second coupler and in this case, with six cascaded couplers, it is multiplied by 32, increasing from 108 MHz to 3.5 GHz. Finally, 7.5 mW of output power from the repetition rate multiplier is polarized with an inline polarization beam splitter (PBS), following a polarization controller. It is then amplified to 300 mW in the first amplifier stage, which comprises 30-cm long core-pumped Yb-doped fiber (Yb-401PM, CorActive, Inc., peak absorption of 570 dB/m at 976 nm) before entering the highly cascaded amplifier system which is same as the section starting with CFBG pulse stretcher in Fig. 6. One full cycle of the repeated pulse train of the oscillator containing 32 (2^5) pulses is shown in Fig. 9(a) where the irregularity in the pulse energy distribution and temporal spacing is limited to $\sim$3%. Fig. 9(b) shows a 20-GHz span of the RF spectrum recorded with 100 kHz resolution bandwidth. The system can amplify 15 ns-long bursts comprising of 50 pulses to a net energy of 215 μJ (Fig. 9(c)), and 230 ns-long bursts of 800 pulses to net energy of 490 μJ (Fig. 9(d)) at a burst repetition rate of 1 kHz.

E. The First Compact Laser System for the Ablation-Cooled Laser-Material Processing

Having demonstrated a new regime of laser-material processing which opens the door to the simplification of ultrafast lasers
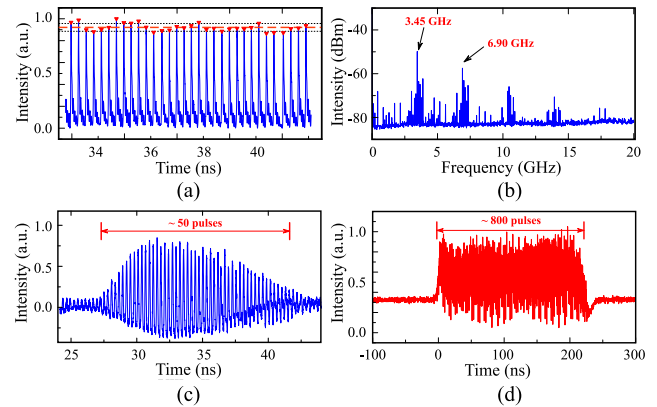

Fig. 9. (a) Temporal profile of 3.5-GHz pulse train measured after the repetition rate multiplier. (b) Measured RF spectrum with 20 GHz span and 100 kHz resolution. (c) Measured output pulse train for the 15 ns-long burst after dechirping. (d) 230 ns-long burst train containing approximately 800 pulses. Reproduced with permission from [21], ©2016 Elsevier Publishing Group.
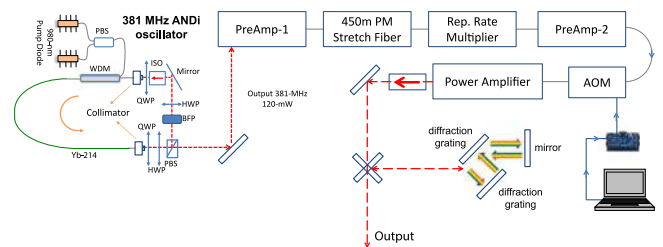

Fig. 10. Schematic diagram of the first compact fiber amplifier system built to verify ablation-cooled laser material removal with the oscillator given in detail. WDM: wavelength division multiplexer; PBS: polarization beam splitter, QWP: quarter-wave plate, HWP: half-wave plate, BFP: birefringent filter plate, ANDi: all-normal dispersion, PM: polarization maintaining, AOM: acousto-optic modulator. Inset: Photograph of the oscillator.

used for material ablation, we developed a compact all-PM-fiber laser amplifier system with an intraburst repetition rate of 1.6 GHz on a 40 × 65 cm platform to verify our claim (Fig. 10). The seed signal is generated by a home-built ANDi oscillator with a repetition rate of 381 MHz (left side of Fig. 10), which we believe to be the highest value demonstrated for an ANDi laser up to date. The oscillator is pumped by two 400-mW single-mode diodes coupled by a polarization beam splitter into a WDM and consists of 40 cm fiber and 18 cm free space sections overall. The 100 mW signal taken from the beam splitter in the free space section has a spectrum centered at 1035 nm and 16 nm FWHM. Rest of the system is built of polarization maintaining (PM) components, and following the oscillator seed signal is amplified by a single-mode pre-amplifier which controls both dispersion and nonlinearity in the amplifier system. The pulses are stretched with an 110 m-long fiber after this pre-amplifier and raised to a repetition rate of 1.5 GHz by a cascaded multiplier similar to the one shown in Fig. 8, except with three stages instead of six. The signal is amplified again by a second single-mode pre-amplifier to an average power of 425 mW before transformed into burst-mode via an acousto-optic modulator (AOM). Finally, a forward-pumped double-clad power amplifier, built of PM 20/125 Yb 1200 DC (nLight) fiber and

pumped by an 18-W wavelength stabilized diode, boosts the optical power. Fiber lengths are shortened as much as possible to minimize nonlinear effects including Raman scattering, and thus the power conversion efficiency is relatively low, around 20% for the power amplifier. Nevertheless, the amplification level in the power amplifier is remarkably high, and to be specific, for 80-pulse bursts at 25 kHz burst repetition rate, ~0.3 mW signal is boosted to nearly 3 W by a mere 40 dB. Pulses of 1.4 μJ are compressed down to 270 fs via 1200 line/mm transmission gratings with an efficiency of 70%. The system can produce up to 2 W at the compressor output where for 25 kHz burst repetition rate this yields 1 μJ individual pulse energy with 80-pulse bursts and for 200 kHz 0.4 μJ individual pulse energy with 20-pulse bursts.

This system was tested in glass processing which requires high peak powers, and ablation threshold of 300 nJ pulse energy was obtained with 270 fs pulses and 20 μm spot size (diameter) using bursts of 80, 100, and 200 pulses, each repeated at 25 kHz. Comparing to published results [36]–[38], we achieved an improvement of 12 to 20 times in threshold fluence and 17 to 1000 times in threshold intensity.

III. HIGH-POWER SYSTEMS

So far, we presented fiber lasers generating high pulse energies at low burst repetition rates, corresponding to modest few-watt-level average powers. In some applications, much higher repetition rates and correspondingly higher average powers are demanded, and when accompanied by high scan speeds high power lasers hold the potential to reach high ablation rates required for industrial scale material processing. Hence, high power fiber lasers have been developed significantly and presented in many excellent articles [1], [2], [4], [39]–[48]. In such systems, peak power and average power levels are limited by nonlinear and thermal effects which need to be managed to improve power handling [49]–[52]. In our journey to develop high power and high repetition rate ultrafast fiber laser systems, we first tackled the thermal management and nonlinearity issues mainly, targeting 100 W level with a continuously repeated pulsed system while keeping the pulse energy at modest levels of μJ. Thereafter, we continued by implementing burst mode to obtain higher pulse energy levels.

A. 100-MHz 100-W Yb All-Fiber Doping-Managed Laser System

Obtaining high average power and high peak energy pulses simultaneously requires competing solutions. In order to partially mitigate this trade-off, we proposed doping management which implies the use of a combination of fibers with different doping levels for the amplification scheme. The concept of doping management was developed with the aid of numerical simulations for amplifier gain used to determine heat load and for pulse propagation used to determine nonlinear phase shift. While gain simulation utilizes wavelength-dependent emission and absorption cross-sections, pulse propagation simulation is based on nonlinear Schrödinger equation (see [30], [53] for more details). Ideally, the doping level should increase smoothly such
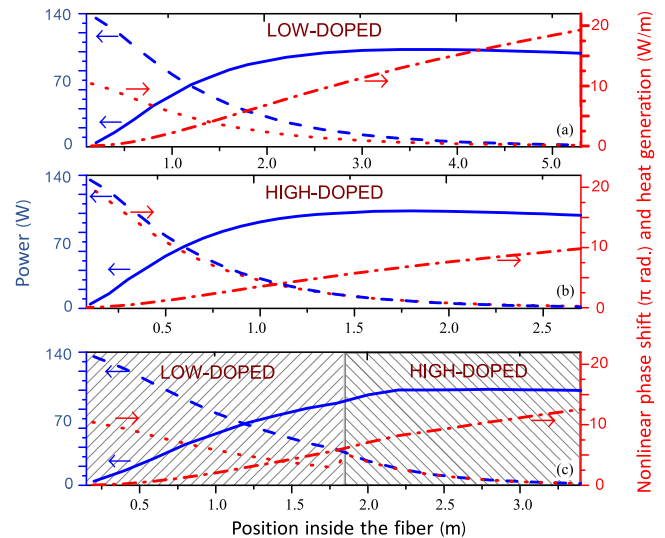

Fig. 11. Simulated evolution of signal (solid curve) and pump (dashed curve) power, nonlinear phase shift (dot-dashed curve) and heat generation per unit length (dotted curve) along (a) low-doped, (b) high-doped, (c) low- and high-doped, hybrid gain fibers. Reproduced with permission from [22], ©2012 OSA Publishing Group.

that heat generation per unit length is kept close to, but below a safe level. Since fibers with continuously changing doping concentrations are not available, we focussed on the use of two segments of fiber with different doping levels, spliced together. Fig. 11 shows simulation results of the pump and signal powers, as well as heat generation per unit length and accumulated nonlinear phase shift for three amplifier configurations: (i) with low-doped fiber (doping concentration of 5×10^{25} m^{-3}, (ii) with high-doped fiber (doping concentration of 1×10^{26} m^{-3}), (iii) with a segment of low-doped fiber, followed by a segment of high-doped fiber (i.e., implementing discrete doping management). Note that, the hybrid amplifier emerges as a superior configuration with the maximum heat generation equal to that of the low-doped fiber, at 10 W/m, and the nonlinear phase shift of 12.5π, representing only a small increase compared to the high-doped amplifier.

Encouraged by the simulation results, we developed the first fiber laser-amplifier system which has the last stage built of hybrid gain fiber composed of high-doped and low-doped Yb fibers [22] (Fig. 12). The amplifier generates 100 W at 100 MHz yielding pulse energy of 1 μJ. The seed oscillator is a 100-MHZ passively mode locked all-normal dispersion (ANDi) laser. The amplifier comprises three stages, which are all-fiber-integrated, delivering 13 ps pulses at full power. In the final power amplifier stage, the first gain segment is a 1.8 m-long low-doped double-clad Yb-fiber (Yb-700 25/250-DC) with 2.5 dB/m cladding absorption at 976 nm and the second segment is a 1.6 m-long high-doped Yb fiber(Yb-1200 25/250-DC) with 3.5 dB/m cladding absorption at 976 nm. A (6 + 1)×1 pump-signal combiner is used to deliver pump light from six 25-W fiber-pigtailed diode lasers and boost the 1-W input seed up to 100 W [22]. Prechirping is implemented where a grating compressor (1200 line/mm) after the first stage single-mode amplifier is used to control the chirp of the seed pulses to obtain the shortest pulse duration of
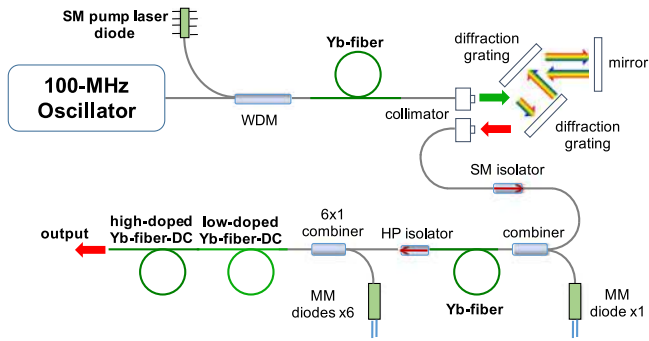
Fig. 12.   Schematic of the 100-W average power fiber laser system using doping management. WDM: Wavelength division multiplexer, SM diode: single mode diode, MM diode: Multi mode diode, SM isolator: single mode isolator, MM isolator: Multimode isolator, MPC: Multimode pump-signal combiner, DC: double-clad. Reproduced with permission from [22], ©2012 OSA Publishing Group.

4.5 ps, at a total GDD of -0.12 ps^2 for the overall laser-amplifier system. Hence, ∼200 kW peak power 1 μJ pulses are generated at the output without using external pulse compression.

B. 100 W, Burst-mode, Doping-Managed Yb Fiber Amplifier

We next developed this system into the first high power burst-mode fiber laser system, generating 100-W average power with 10-μJ individual pulse and 100-μJ burst energy (1 MHz burst repetition rate), scaling the burst-mode operation of fiber amplifiers from the ∼1-W level to 100-W level. [23]. The system was designed to generate sub-20 ps pulses directly to avoid the use of external compression, which is costly and challenging at 100 W. Negative prechirping was employed to control chirp of the pulses as they traverse through the final amplifier, initially undergoing self-similar amplification [54], [55], compensating for part of the nonlinear effects, before spectral broadening due to Raman scattering begins to dominate. The schematic of the laser setup is similar to Fig. 12 (see for details [23]) except that a fiber-coupled acousto-optic modulator (AOM) is added at the output of the oscillator to generate 10-pulse bursts at 1 MHz. Because of the high burst repetition rate at 1 MHz, amplified spontaneous emission between the bursts is negligible; therefore, continuous pumping is utilized leading to homogenous energy distribution inside bursts with no need for pre-shaping. The total length of the fibers in this system is 134 m, and grating dispersion is set to −2.56 ps^2 via prechirping at the input of the final amplifier. Thus the shortest output pulse duration is obtained at full power where the total group dispersion delay is adjusted to a calculated value of 0.16 ps^2.

The measured autocorrelation signals are presented in Fig. 13(a). The pulse widths are inferred to be 7, 14 and 17 ps at 20, 60 and 100 W output powers, respectively. Fig. 13(b) shows measured optical spectra in linear scales for 20, 60 and 100 W output power, corresponding to 2 μJ, 6 μJ and 10 μJ individual pulse energies, respectively. The corresponding spectral widths (measured at -3 dB) are 110 nm, 200 nm, and 240 nm, respectively. Fig. 13(c) presents the variation of output spectral and pulse width of power amplifier versus output power.
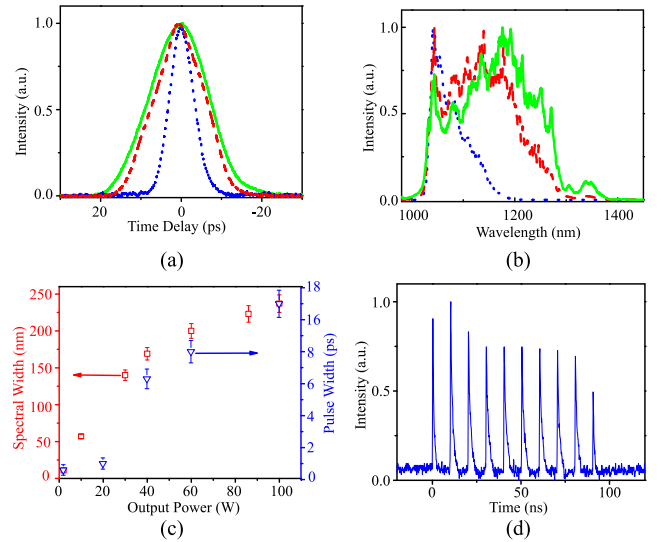

Fig. 13.   (a) Measured intensity autocorrelation burst mode operation at output powers of 20 W (dotted line), 60 W (dashed line), and 100 W (solid line). (b) Measured optical spectra in burst mode operation at output powers of 20 W (dotted line), 60 W (dashed line), and 100 W (solid line). (c) Spectra width (squares) and pulse width (down-pointing triangles) versus output power. (d) Pulse train in one burst from power amplifier at 100 W output power. The pulse energy variation is −17%. Reproduced with permission from [23], ©2014 OSA Publishing Group.
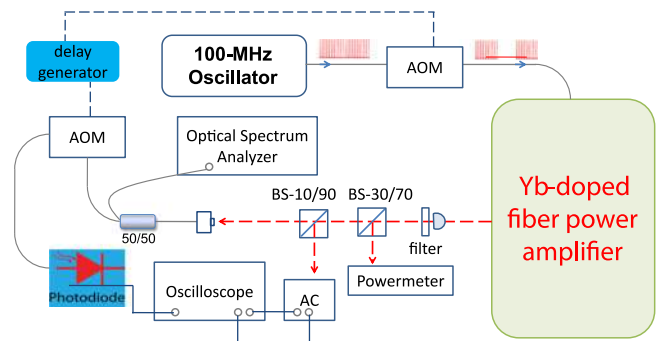

Fig. 14.   Schematic of ASE measurement setup. OSA, optical spectrum analyzer; OSC, oscilloscope; AC, auto correlator; BS, beam splitter; AOM; acousto-optic modulator. Reproduced with permission from [24], ©2015 OSA Publishing Group.

The pulse burst generated from the power amplifier at 100 W (Fig. 13(d)) has an energy of 100 μJ where the average individual pulse energy is 10 μJ. The largest (smallest) pulse energy in the burst is ∼13 μJ (∼7 μJ). and the standard deviation is calculated to be 17%.

C. Investigation of ASE in Continuous-Pumped High Power Systems and Reaching 145 W Burst-Mode Output

In order to investigate ASE generated between bursts in continuous-pumping systems, a measurement setup (Fig. 14) was realized to monitor detailed system characteristics simultaneously (see [24] for more details), as well as to measure ASE content directly in the time domain as first described in [56]. In order to rule out any indirect influence of nonlinear effects on the
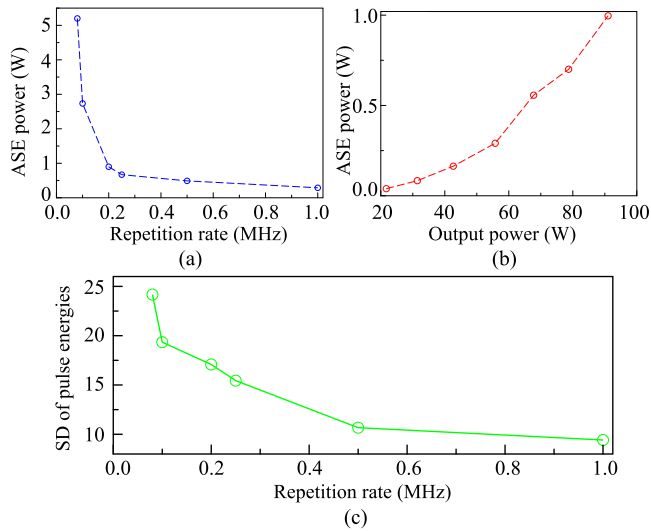
Fig. 15. (a) Measured ASE power as a function of burst repetition rate at 50 W output. (b) Measured ASE power versus output power, for which the burst repetition rate was kept at 1 MHz. (c) Standard deviation (SD) of pulse energies within the pulse bursts as a function of burst repetition rate measured at 50 W. Reproduced with permission from [24], ©2015 OSA Publishing Group.

ASE measurements, which could occur due to, e.g., changes in efficiency due to Raman-induced red-shifting of the spectrum, the (average) pulse energy was kept constant (5 μJ). This was achieved by adjusting the number of pulses per burst between 10 and 125, corresponding to burst energies ranging from 50 μJ to 625 μJ and burst repetition rates ranging from 1 MHz to 80 kHz, respectively.

In continuous pumping at 50-W output power, experimental measurements show that the ASE power between bursts is lower than 0.5 W for burst repetition rates above 200 kHz and rises sharply for below 200 kHz (Fig. 15(a)). The ASE increases linearly with output power as is shown in Fig. 15(b). Interpolation of the data in Fig. 15(b) up to higher powers indicates that pulsed pumping is unnecessary as long as the bursts are repeated at 200 kHz or higher, even for 150 W, which allows for substantial simplification of the setup. Fig. 15(c) shows the measured pulse energy variation across the burst for different burst repetition rates. This variation can be compensated for by preshaping the burst envelope [19] at the cost of increased complexity in control electronics. However, at burst repetition rates above 500 kHz, the standard deviation of the pulse energy within a burst is less than ~10%.

Aided by the results of our ASE investigation, we upgraded the high-power burst-mode fiber laser by adding two preamplifiers to reach 145-W average power at a burst repetition rate of 1 MHZ generating 100-ns-long 10-pulse bursts [24]. Similar to [23], we employed pre-chirping and achieved 13-ps long pulses directly from the fiber laser. The measured optical spectrums for 50, 100 and 145 W output power, corresponding to 5, 10 and 14.5 μJ individual pulse energy, respectively are shown in Fig. 16(a) and (b). Four-wave mixing and intra-pulse Raman scattering lead to spectral broadening and red-shifting substantially with increasing pulse energy as shown in these figures. The measured autocorrelation signal is presented in Fig. 16(c),
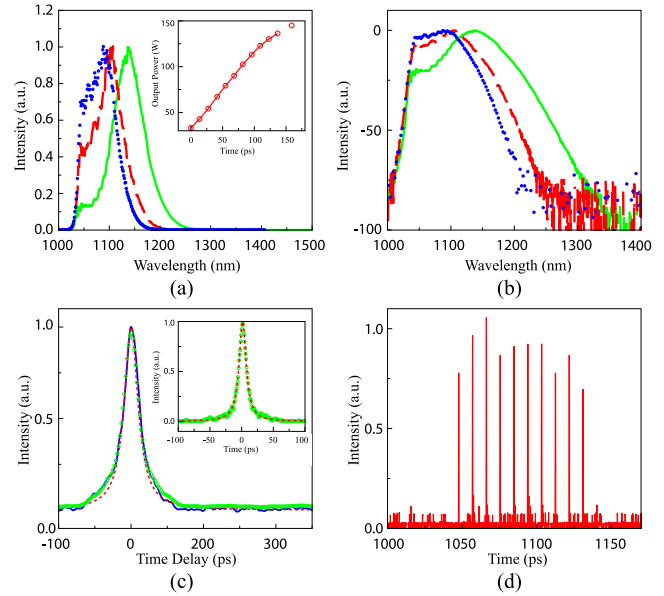

Fig. 16. (a) Measured output spectra in burst mode operation at output powers of 50 W (blue-dotted line), 100 W (red-dashed line) and 145 W (green-solid line). Inset: Measured output power versus pump power. (b) Measured output spectra in semi-logarithmic version. (c) Measured intensity autocorrelation at 145 W of output power (blue-solid line) along with retrieved autocorrelation trace obtained using PICASO (green circles) and Lorentzian fit (red-dashed line). Inset: Retrieved pulse shape (green circles) and Lorentzian fit (red-dashed line) with FWHM of 12 ps. (d) Pulse train in one burst from power amplifier at 145 W output power. Reproduced with permission from [24], ©2015 OSA Publishing Group.
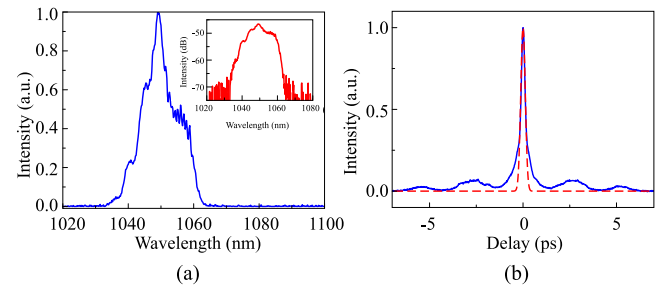

Fig. 17. (a) Measured optical spectrum in the burst mode operation at output power of 50 W. Inset: in semi-logarithmic version. (b) Measured intensity autocorrelation at 50 W of output power (blue-solid line) along with Gaussian fitting (red dashed-line) indicates a pulse width of 260 fs.

fitted by a Lorentzian pulse intensity shape, which provides a better fit than the commonly used Gaussian shape. The inferred full-width half-maximum (FWHM) pulse duration is 12.8 ps. We also used the PICASO algorithm [57] to fit the measured autocorrelation and optical spectrum with an arbitrary spectral phase profile, from which the inferred FWHM pulse duration was 12 ps (inset of Fig. 16(c)).

At the highest power of 145 W, the estimated nonlinear phase shift in the last stage of amplification is about 180π. The resulting spectral evolution is dominated by Raman scattering, as evidenced by the asymmetric growth of the spectrum towards longer wavelengths. However, there is a complex interplay between Raman scattering, SPM, and higher-order dispersion, while soliton-like effects that typically underlie
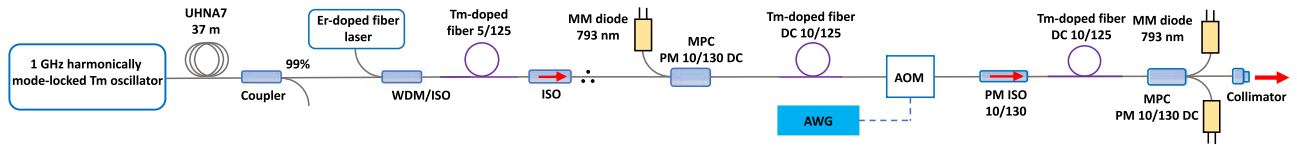
Fig. 18.   Schematic diagram of the Tm-fiber burst-mode laser system. WDM: wavelength division multiplexer, MM: multi-mode, ISO: isolator, MPC: multimode pump-signal combiner, DC: double-clad, PM: polarization maintaining, AOM: acousto-optic modulator, AWG: arbitrary waveform generator.

similar spectral enhancements do not play a significant role, since the fibers have normal dispersion and the pulses are positively chirped in the regions where nonlinearity is the strongest. As to be expected, there is a trade-off between nonlinear spectral reshaping and pulse duration, similar to the results in [22]. If the launched pulses are more heavily chirped, nonlinear effects are reduced, but this results in longer pulses. For shorter launched pulse durations, nonlinear spectral broadening leads to additional dispersive stretching. Thus, the pulse duration becomes clamped. However, by implementing doping management with a third segment with even higher doping level (increasing the gain/length), gain filtering can be exploited to reduce pulse durations to sub-10 ps.

D. High-Power GHz Intraburst Fiber Laser System

We developed a 50-W fiber laser system to test the ablation-cooled laser material removal principle in the high power applications. This is a burst mode all-fiber laser system with 1.6 GHz intraburst and 200-kHz burst repetition rate generating 250 μJ and 0.4 μJ, burst and pulse energy, respectively.

The 100 MHz oscillator generates 4-ps long pulses which proceed to a repetition rate multiplier built of five stages of 50/50 couplers similar to the one shown in (Fig. 8). After stretching via 57-m long fiber, the 5-mW signal containing 90-ps long pulses at 1.6 GHz repetition rate is amplified to 112 mW in the first stage of the amplifier. An acousto-optic modulator is employed to generate the bursts. Second stage amplifier raises the output signal from acousto-optic modulator to about 190 mW. The power amplifier is based on 4-m long Yb 30/250-DC with 3.5 dB/m cladding absorption at 976 nm. This amplifier stage is pumped by four 25 W diode by a high-power multimode pump-signal combiner (MPC). A high power isolator-collimator at the exit of the amplifier delivers the 50 W output with a spectrum centered at 1050 nm and width of 10 nm (Fig. 17(a)) to a 1200 l/mm transmission grating pair where compressed pulses of 260 fs duration (Fig. 17(b)) are obtained.

IV. FIRST TM-DOPED ULTRAFAST BURST-MODE LASER SYSTEM WITH GHZ INTRABURST REPETITION RATE

We believe that ablation-cooled laser material regime has a big potential for medical surgery in the vicinity of 1.94 μm where a local absorption peak of water exists [28] which significantly enhances laser interaction with water-rich soft tissues. In case this potential is realized, boosting ablation speed with minimal collateral damage and heating can have a major impact on microsurgery in terms of operational speed and precision, and simplification of ultrafast lasers demanded for such oper-

ations. With the motivation of investigating this potential, we decided to develop high repetition rate all-fiber versions of ultrafast Tm-doped lasers that operate in the 2 μm wavelength range and have current applications such as medical surgery, atmospheric sensing, spectroscopy, and processing of polymers [58], [59]. To this end, we developed an ultrafast all-fiber Tm-doped burst-mode laser system with GHz intraburst repetition rate operating at 2 μm [27]. The laser amplifier system is seeded by a harmonically mode-locked dispersion-managed oscillator operating at ∼1 GHz repetition rate and can produce 500-pulse bursts at a repetition rate of 50 kHz and an average output power of 1 W. 40-nJ pulses with 340 fs width are obtained directly at the output of the amplifier which is made possible by the overall dispersion-managed architecture. The thulium-fiber laser system, shown schematically in Fig. 18, consists of an all-fiber dispersion-managed oscillator, followed by three stages of amplification and a fiber-coupled acousto-optic modulator (AOM) located before the final amplifier which imposes the burst-mode on the pulse train. The oscillator cavity has a net dispersion of -0.062 ps^2 and a fundamental repetition rate of 107.6 MHz. The repetition rate shifts to higher harmonics by boosting the pump power and adjusting the polarization controllers. Stable operation is obtained at the 9th harmonic (970 MHz) when the pump power is increased to 1.05 W from 470 mW at the fundamental. Dispersion management is implemented with the guidance of the pulse propagation simulation based on the extended nonlinear Schrödinger equation (further described in [53]). Thereby, optimizing the length of the positive dispersion stretch fiber (UHNA7), the seed pulses of 1.5 ps are stretched to ∼40 ps and compressed to 340 fs in the following segments of SMF 28 and Tm-doped fibers with anomalous dispersion.

V. CONCLUSION

In this report, we have provided a review of our developmental work in building high repetition rate fiber laser systems for ultrafast material processing, covering the period of last seven years. It all began with the idea of sending ultrafast pulses to a material at such a high repetition frequency that as the ablation takes place, the energy which is deposited on the material does not have the time to diffuse away from the targeted spot and is highly localized. Hence the ablation occurs in a sort of supersonic manner. To investigate this idea, we went on to develop high repetition rate ultrafast laser systems with integrated fiber architecture which provide stability and versatility that processing demands. Further, we implemented burst-mode to reach high energy pulses at high repetition rates with duty cycles low enough that brought power levels within practical

domains. We moved in two main directions; burst-mode laser systems with effectively low repetition rates to obtain high pulse energies on the level of tens of μJ's with W level power output and high power systems in the 50 to 150 W power range with effective repetition rates above MHz. During the course of this work, we demonstrated the first burst-mode fiber laser system, able to produce 250 μJ bursts containing 20 μJ individual pulses compressible to ∼400 fs, high-level homogenization of intraburst energy with in-house developed pre-shaping and control electronics, and the first high power fiber amplifier system with hybrid doping concentration. Further, investigation of ASE generation in pulse-pumped and continuous-pumped amplifier systems shed light on the limits of fiber burst-mode amplification. In the limits, we increased the intraburst repetition rate to 3.5 GHz and average power to 145 W. Meanwhile, using the laser systems we developed, we were able to verify our idea of supersonic ablation and establish the new regime of ultrafast material processing which we called ablation-cooled laser material removal [5]. We further built the first fiber laser systems, one low power and one high power, based on the ablation-cooled removal principle. Finally, we started to develop high intraburst repetition rate Tm-doped systems operating near 2 μm, to exploit this principle in tissue processing.

REFERENCES

[1] D. J. Richardson, J. Nilsson, and W. A. Clarkson, "High power fiber lasers: Current status and future perspectives [Invited]," *J. Opt. Soc. Amer. B*, vol. 27, pp. B63–B92, 2010.

[2] J. Nilsson and D. N. Payne, "High-power fiber lasers," *Science*, vol. 332, pp. 921–922, 2011.

[3] M. E. Fermann and I. Hartl, "Ultrafast fibre lasers," *Nature Photon.*, vol. 7, pp. 868–874, 2013.

[4] C. Jauregui, J. Limpert, and A. Tünnermann, "High-power fibre lasers," *Nature Photon.*, vol. 7, pp. 861–867, 2013.

[5] C. Kerse *et al.*, "Ablation-cooled material removal with ultrafast bursts of pulses," *Nature*, vol. 537, pp. 84–88, 2016.

[6] H. Braun *et al.*, "CLIC 2008 parameters," CERN-OPEN-2008-021, CLIC-NOTE-764, 2008.

[7] I. Will, H. I. Templin, S. Schreiber, and W. Sandner, "Photoinjector drive laser of the FLASH FEL," *Opt. Express*, vol. 19, pp. 23770–23781, 2011.

[8] P. Wu, W. R. Lempert, and R. B. Miles, "Megahertz pulse-burst laser system and visualization of shock-wave/boundary-layer interaction," *AIAA J.*, vol. 38, pp. 672–679, 2000.

[9] B. S. Thurow, A. Satija, and K. Lynch, "Third-generation megahertz-rate pulse burst laser system," *Appl. Opt.*, vol. 48, pp. 2086–2093, 2009.

[10] D. J. Den Hartog *et al.*, "Pulse-burst laser systems for fast Thomson scattering (invited)," *Rev. Sci. Instrum.*, vol 81, 2010, Art. no. 10D513.

[11] M. Murakami *et al.*, "Burst-mode femtosecond pulsed laser deposition for control of thin film morphology and material ablation," *Appl. Phys. Express*, vol. 2, 2009, Art. no. 042501.

[12] T. Liu, J. Wang, G. I. Petrov, V. V. Yakovlev, and H. F. Zhang, "Photoacoustic generation by multiple picosecond pulse excitation," *Med. Phys.*, vol. 37, pp. 1518–1521, 2010.

[13] W. Hu, Y. C. Shin, and G. King, "Modeling of multi-burst mode picosecond laser ablation for improved material removal rate," *Appl. Phys. A, Mater. Sci. Process.*, vol. 98, pp. 407–415, 2010.

[14] R. Knappe, H. Haloui, A. Seifert, A. Weis, and A. Nebel, "Scaling ablation rates for picosecond lasers using burst micromachining," *Proc. SPIE*, vol. 7585, 2010, Art. no. 75850H.

[15] R. S. Marjoribanks *et al.*, "Ablation and thermal effects in treatment of hard and soft materials and biotissues using ultrafast-laser pulse-train bursts," *Photon. Lasers Med.*, vol. 1, pp. 155–169, 2012.

[16] Z. Qian *et al.*, "Pulsetrain-burst mode, ultrafast-laser interactions with 3D viable cell cultures as a model for soft biological tissues," *Biomed. Opt. Express*, vol. 5, pp. 208–222, 2014.

[17] M. Lapczyna, K. P. Chen, P. R. Herman, H. W. Tan, and R. S. Marjoribanks, "Ultra high repetition rate (133 MHz) laser ablation of aluminum with 1.2-ps pulses," *Appl. Phys. A, Mater. Sci. Process.*, vol. 69, pp. S883–S886, 1999.

[18] H. Kalaycioglu, K. Eken, and F. Ö. Ilday, "Fiber amplification of pulse bursts up to 20 μJ pulse energy at 1 kHz repetition rate," *Opt. Lett.*, vol. 36, pp. 3383–3385, 2011.

[19] H. Kalaycıoğlu *et al.*, "1-mJ pulse bursts from a Yb-doped fiber amplifier," *Opt. Lett.*, vol. 37, pp. 2586–2588, 2012.

[20] H. Kalaycıoğlu, O. Akcaalan, S. Yavas, Y. B. Eldeniz, and F. Ö. Ilday, "Burst-mode Yb-doped fiber amplifier system optimized for low-repetition-rate operation," *J. Opt. Soc. Amer. B*, vol. 32, pp. 900–906, 2015.

[21] C. Kerse, H. Kalaycıoğlu, P. Elahi, Ö. Akcaalan, and F. Ö. Ilday, "3.5-GHz intraburst repetition rate ultrafast Yb-doped fiber laser [Invited]," *Opt. Commun.*, vol. 366, pp. 404–409, 2016.

[22] P. Elahi *et al.*, "Doping management for high-power fiber lasers: 100 W, few-picosecond pulse generation from an all-fiber-integrated amplifier," *Opt. Lett.*, vol. 37, pp. 3042–3044, 2012.

[23] P. Elahi, S. Yilmaz, Y. B. Eldeniz, and F. Ö. Ilday, "Generation of picosecond pulses directly from a 100 W, burst-mode, doping-managed Yb-doped fiber amplifier," *Opt. Lett.*, vol. 39, pp. 236–239, 2014.

[24] S. Yilmaz, P. Elahi, H. Kalaycıoğlu, and F. Ö. Ilday, "Amplified spontaneous emission in high-power burst-mode fiber lasers," *J. Opt. Soc. Amer. B*, vol. 32, pp. 2462–2466, 2015.

[25] S. Breitkopf *et al.*, "58 mJ burst comprising ultrashort pulses with homogenous energy level from an Yb-doped fiber amplifier," *Opt. Lett.*, vol. 37, pp. 5169–5171, 2012.

[26] X. Li, S. Zhang, Y. Hao, and Z. Yang, "Pulse bursts with a controllable number of pulses from a mode-locked Yb-doped all fiber laser system," *Opt. Express*, vol. 22, pp. 6699–6706, 2014.

[27] P. Elahi, H. Kalaycıoğlu, Ö. Akçaalan, and F. Ö. Ilday, "Burst-mode thulium fiber laser delivering femtosecond pulses with 1-GHz intraburst repetition rate," *Opt. Lett.*, vol. 42, pp. 3808–3811, 2017.

[28] J. A. Curcio and C. C. Petty, "The near infrared absorption spectrum of liquid water," *J. Opt. Soc. Amer.*, vol. 41, pp. 302–304, 1951.

[29] F. Ö. Ilday, H. Lim, J. Buckley, and F. W. Wise, "Practical, all-fiber source of high-power, 120-fs pulses at 1 micron," *Opt. Lett.*, vol. 28, pp. 1362–1364, 2003.

[30] P. K. Mukhopadhyay, K. Özgören, I. L. Budunoglu, and F. Ö. Ilday, "All-fiber low-noise high-power femtosecond Yb-fiber amplifier system seeded by an all-normal dispersion fiber oscillator," *IEEE J. Sel. Topics Quantum Electron.*, vol. 15, no. 1, pp. 145–152, Jan. 2009.

[31] A. Chong, J. Buckley, W. Renninger, and F. W. Wise, "All-normal-dispersion femtosecond fiber laser," *Opt. Express*, vol. 14, pp. 10095–10100, 2006.

[32] A. Winter *et al.*, "Towards high-performance optical master oscillators for energy recovery linacs," *Nucl. Instrum. Methods Phys. Res. A, Accel. Spectrom. Detect. Assoc. Equip.*, vol. 557, pp. 299–304, 2006.

[33] S.-S. Min, Y. Zhao, and S. Fleming, "Repetition rate multiplication in figure-eight fibre laser with 3 dB couplers," *Opt. Commun.*, vol. 277, pp. 411–413, 2007.

[34] A. Haboucha *et al.*, "Optical-fiber pulse rate multiplier for ultralow phase-noise signal generation," *Opt. Lett.*, vol. 36, pp. 3654–3656, 2011.

[35] R. Maram, J. Van Howe, M. Li, and J. Azaa, "Lossless fractional repetition-rate multiplication of optical pulse trains," *Opt. Lett.*, vol. 40, pp. 375–378, 2015.

[36] A. Ben-Yakar and R. L. Byer, "Femtosecond laser ablation properties of borosilicate glass," *J. Appl. Phys.*, vol. 96, pp. 5316–5323, 2004.

[37] C. B. Schaffer, A. Brodeur, J. F. Garca, and E. Mazur, "Micromachining bulk glass by use of femtosecond laser pulses with nanojoule energy," *Opt. Lett.*, vol. 26, pp. 93–95, 2001.

[38] E. Bulushev, V. Bessmeltsev, A. Dostovalov, N. Goloshevsky, and A. Wolf, "High-speed and crack-free direct-writing of microchannels on glass by an IR femtosecond laser," *Opt. Lasers Eng.*, vol. 79, pp. 39–47, 2016.

[39] M. N. Zervas and C. A. Codemard, "High power fiber lasers: A review [Invited]," *IEEE J. Sel. Topics Quantum Electron.*, vol. 20, no. 5, Sep./Oct. 2014, Art. no. 0904123.

[40] J. Limpert *et al.*, "High repetition rate gigawatt peak power fiber laser-systems: Challenges, design, and experiment," *IEEE J. Sel. Topics Quantum Electron.*, vol. 15, no. 1, pp. 159–169, Jan. 2009.

[41] T. Eidam *et al.*, "Fiber chirped-pulse amplification system emitting 3.8 GW peak power," *Opt. Express*, vol. 19, pp. 255–260, 2011.

[42] S.-P. Chen, H.-W. Chen, J. Hou, and Z.-J. Liu, "100 W all fiber picosecond MOPA laser," *Opt. Express*, vol. 17, pp. 24008–24012, 2009.

[43] K. K. Chen *et al.*, "Polarisation maintaining 100W Yb-fiber MOPA producing μJ pulses tunable in duration from 1 to 21 ps," *Opt. Express*, vol. 18, pp. 14385–14394, 2010.

[44] Z. Zhao, B. M. Dunham, I. Bazarov, and F. W. Wise, "Generation of 110 W infrared and 65 W green power from a 1.3-GHz sub-picosecond fiber amplifier," *Opt. Express*, vol. 20, pp. 4850–4855, 2012.

[45] K.-H. Hong *et al.*, "Generation of 287 W, 5.5 ps pulses at 78 MHz repetition rate from a cryogenically cooled Yb:YAG amplifier seeded by a fiber chirped-pulse amplification system," *Opt. Lett.*, vol. 33, pp. 2473–2475, 2008.

[46] P. Dupriez *et al.*, "321 W average power 1 GHz, 20 ps, 1060 nm pulsed fiber MOPA source," in *Proc. Opt. Fiber Commun. Conf.*, Anaheim, CA, USA, 2005, Paper PDP3.

[47] F. Harth *et al.*, "High power laser pulses with voltage controlled durations of 400–1000 ps," *Opt. Express*, vol. 20, pp. 7002–7007, 2012.

[48] E. Lippert, S. Nicolas, G. Arisholm, K. Stenersen, and G. Rustad, "Mid-infrared laser source with high power and beam quality," *Appl. Opt.*, vol. 45, pp. 3839–3845, 2006.

[49] X. Liu, M. H. Hu, C. G. Caneau, R. Bhat, and C.-E. Zah, "Thermal management strategies for high power semiconductor pump lasers," *IEEE Trans. Compon. Packag. Technol.*, vol. 29, no. 2, pp. 268–276, Jun. 2006.

[50] Y. Fan *et al.*, "Thermal effects in kilowatt all-fiber MOPA," *Opt. Express*, vol. 19, pp. 15162–15172, 2011.

[51] Y. Wang, C. Q. Xu, and H. Po, "Thermal effects in kilowatt fiber lasers," *IEEE Photon. Technol. Lett.*, vol. 16, no. 1, pp. 63–65, Jan. 2004.

[52] G. P. Agrawal, "Nonlinear fiber optics: Its history and recent progress [Invited]," *J. Opt. Soc. Amer. B*, vol. 28, pp. A1–A10, 2011.

[53] B. Oktem, C. Ülgüdür, and F. Ö. Ilday, "Soliton-similariton fibre laser," *Nature Photon.*, vol. 4, pp. 307–311, 2010.

[54] M. E. Fermann, V. I. Kruglov, B. C. Thomsen, J. M. Dudley, and J. D. Harvey, "Self-similar propagation and amplification of parabolic pulses in optical fibers," *Phys. Rev. Lett.*, vol. 84, pp. 6010–6013, 2004.

[55] D. B. Soh, J. Nilsson, and A. B. Grudinin, "Efficient femtosecond pulse generation using a parabolic amplifier combined with a pulse compressor. II. Finite gain-bandwidth effect," *J. Opt. Soc. Amer. B*, vol. 23, pp. 10–19, 2006.

[56] I. Pavlov, E. Dülgergil, E. Ilbey, and F. Ö. Ilday, "Diffraction-limited, 10-W, 5-ns, 100-kHz, all-fiber laser at 1.55 μm," *Opt. Lett.*, vol. 39, pp. 2695–2698, 2014.

[57] J. W. Nicholson, J. Jasapara, W. Rudolph, F. G. Omenetto, and A. J. Taylor, "Full-field characterization of femtosecond pulses by spectrum and cross-correlation measurements," *Opt. Lett.*, vol. 24, pp. 1774–1776, 1999.

[58] K. Scholle, S. Lamrini, P. Koopmann, and P. Fuhrberg, "2 μm laser sources and their possible applications," in *Frontiers in Guided Wave Optics and Optoelectronics*, B. Pal, Ed. Rijeka, Croatia: InTech, 2010, pp. 471–500.

[59] J. Geng, Q. Wang, and S. Jiang, "2 μm fiber laser sources and their applications," *Proc. SPIE*, vol. 8164, 2011, Art. no. 816409.

Hamit Kalaycıoğlu received the B.S. degree in applied and engineering physics from Cornell University, Ithaca, NY, USA, in 1987, the M.S. degree in optics from the University of Rochester, Rochester, NY, USA, in 1989, and the Ph.D. degree in electrical engineering from Koç University, Istanbul, Turkey, in 2008. From 1992 to 1993, he was a Research Engineer of infrared imaging and laser systems with the Aselsan, Inc., Ankara, Turkey. From 1993 to 2002, he was in the finance industry, specializing in project finance and financial analysis. He is currently a Senior Research Associate in the Ultrafast Optics and Lasers Laboratory, Bilkent University, Ankara, Turkey.

Parviz Elahi was born in Abadan, Iran, in 1972. He received the B.S. degree in applied physics, the M.S. degree in atomic physics, and the Ph.D. degree in atomic physics, laser, and optics from Shiraz University, Shiraz, Iran, in 1995, 1998, and 2004, respectively. From 2005 to 2010, he was an Assistant Professor of physics at Payame Noor University and Shiraz University of Technology. He is currently a Senior Researcher in the Ultrafast Optics and Laser Laboratory, Bilkent University, Ankara, Turkey. His research interests include ultrafast fiber lasers and laser material processing.

Önder Akçaalan was born in Istanbul, Turkey, in 1987. He received the B.S. degree from Bilkent University, Ankara, Turkey, in 2010, and the M.S. degree from TOBB Economy and Technology University, Ankara, Turkey, in 2013. He is currently a Research Engineer in the Ultrafast Optics and Lasers Laboratory, Bilkent University.

Fatih Ömer Ilday was born in Istanbul, Turkey, in 1976. He received the B.S. degree from Boğaziçi University, Istanbul, Turkey, in 1998, and the Ph.D. degree from Cornell University, Ithaca, NY, USA, in 2003. He was a Postdoctoral Scientist and later a Research Scientist in the Department of Electrical Engineering and Computer Science, Massachusetts Institute of Technology, Cambridge, MA, USA, from 2003 to 2006. In 2006, he joined the Faculty at Bilkent University, Ankara, Turkey, where he is currently an Associate Professor in the Department of Electrical and Electronics Engineering and the Department of Physics.